Predesigned rigid dysprosium(III) single-molecule magnets exhibit preserved superparamagnetism in solution

Xia-Li Ding
Xi'an Jiaotong University
Qian-Cheng Luo
Xi'an Jiaotong University
Yuan-Qi Zhai
Xi'an Jiaotong University
Xu-Feng Zhang
The First Affiliated Hospital of Xi'an Jiaotong University
Yi Lyu
the First Affiliated Hospital of Medical College, Xi'an Jiaotong University https://orcid.org/0000-0003-3636-6664
Xin-Liang Zhang
Honghui Hospital, Xi'an Jiaotong University
Chao Ke
Honghui Hospital, Xi'an Jiaotong University
Yan-Zhen Zheng (zheng.yanzhen@xjtu.edu.cn)
Frontier Institute of Science and Technology (FIST), Xi'an Jiaotong University Shenzhen Research Academy, State Key Laboratory for Mechanical Behavior of Materials, https://orcid.org/0000-0003-4056-097X

Article

Keywords: molecular magnets, lanthanide, complex, superparamagnetism, magnetic liquids

Posted Date: April 28th, 2021

DOI: https://doi.org/10.21203/rs.3.rs-423368/v1

Abstract

Molecules with long preserved magnetic moments are perceived as the smallest units for storing bytes, which could bring a new revolution for information technology. However, the rational design of such molecules remains challenging. Here we show it is possible to predesign such molecules by studying the vibration spectra. Two adamantanol based dysprosium(III) complexes with pentagonal-bipyramidal local geometry were theoretically predicted to display enhanced single-molecule magnet (SMM) behavior due to the reduced vibration modes in low energy regimes. The experimental isolation of these two complexes not only confirms this prediction, but further reveals almost unchanged large energy barriers and high blocking temperatures in solution state. This is never observed in previous studies of SMMs, indicating that the adamantanol ligand is rigid enough to make the complexes exhibiting intrinsic magnetic property in solution. As vibration spectrometer is routinely accessible in common laboratories this work provides a facile strategy to construct high-performance SMMs.

Introduction

The ever increasing demand of faster and smaller data processing devices has pushed the information material close to the regime of quantum effects.[1−3] Single-molecule magnets (SMMs) have been considered such a limit for information storage.[4−9] A molecule being a magnet is due to the magnetic relaxation delayed significantly by a large magnetic anisotropic energy barrier (U_{eff}). If the relaxation time is long enough the magnetization reversal is “blocked” and the characteristic hysteresis effect of a magnet appears.[6−8] The temperature when this effect occurs is called the blocking temperature (T_B). There are three disparate definitions for T_B. The first one is to use the temperature where the maximum zero-field-cooled magnetization appears (T_B^{ZFC}); the second one is the temperature at which the magnetic relaxation time is 100 seconds (T_B^{100s}) and the third one is the highest temperature whenever the magnetic hysteresis is observed (T_B^{H}).[4,10−12] To have wider application temperature T_B should be as high as possible. Right now, the highest T_B^{H} for SMMs is 80 K,[13] just a bit higher than the boiling point of liquid nitrogen.

The key ingredient for high T_B SMMs is to use the dysprosium(III) ion, a heavy lanthanide element with nine unpaired 4f electrons, which has a ground state of $^6H_{15/2}$ with significant magnetic anisotropy.[14−16] With proper axial crystal field U_{eff} of dysprosium(III) based SMMs can be largely enhanced, which now have been widely achieved.[17−20] However, a severe drop of magnetization at zero-field owing to quantum tunneling of magnetization (QTM) remains a challenge for such high barrier SMMs.[21−23] To prevent QTM there are usually two means. The first one is to dilute the sample by doping dysprosium(III) into the diamagnetic matrix of yttrium(III).[24−26] The second one is to employ exchange-coupling interactions of multinuclear complexes to generate a bias field.[27−29] In addition to these two means recently some of us had shown that QTM may correlate to the vibrations of the molecules.[13,30,31] Such a theory was more recently reinforced by functionalization of the axial ligands in the axial positions of a D_{5h} symmetric

molecule-$[Dy(L_4)_2(py)_5][BPh_4]$ **4** (HL_4 = (S)-(-)-1-phenylethanol and py = pyridine). The introduced intra- or inter-molecular C–H•••π and π•••π interactions significantly enhance the stiffness of the moelcular solids, thereby increasing T_B^{100s} up to about 19 K and T_B^H (sweep mode of 10 Oe/s) up to 22 K.[32]

However, we realized that such a success at solid state failed in the solution. As we saw a clear drop of magnetization of the pyridine solution of **4** (**4s**) at zero field and hence, T_B^{100s} of **4s** reduces to only 10 K. This is also observed in the sandwich complex $[Dy(Cp^{ttt})_2][B(C_6F_5)_4]$ **5** which shows high T_B^H of 60 K measured with an average field sweep rate of 22 Oe/s at solid state, but exhibiting a sharply drop of magnetic hysteresis at 2 K in the solution of dichloromethane (**5s**) with T_B^H of 30 K (22 Oe/s).[5] Unfortunately, the solution study of SMMs is still very scarce until now. To the best of my knowledge, there are only two aforementioned examples despite that hundreds of SMMs solids were reported (Table 1). Both **4s** and **5s** show dramatically deteriorated magnetic blocking at zero field, implying that the local environment of the molecule, in particular those governed by intra- and inter-molecular interactions, plays a crucial role in the magnetic dynamics of SMMs.[33–36]

For above reasons, we perceived the solution state of a SMM reflects more of the molecule's intrinsic property. If a molecule is rigid and stable enough, its solid state magnetic ability should be largely retained the same in solution. Given that, we ascribed the serious QTM at zero field of **4s** contrasted with **4** to the "dissolved" intermolecular C–H•••π and π•••π interactions and the relaxed intramolecular C–H•••π interactions. Severe molecular motion can hasten the QTM effect even at solid state. This is also exemplified by the D_{5h} symmetric SMM $[Dy(OCMe_3)_2py_5]BPh_4$ (**3**), which reveals a high U_{eff} of 1815 K only with T_B^{ZFC} of 14 K and $T_B^{100s} \approx 12$ K owing to the highly disordered tert-butyl group in axial sites of the complex.[37] While according to theoretical analysis these motions are just in fingerprints regions of infrared spectra),[38,39] so we expect that by studying the vibration modes of the organic ligands and the complexes can predict the performance of SMMs.

Table 1
Magnetic relaxation parameters of representative high-performance SMMs, H_c represents the coercivity and M_r represents the remanent magnetism.

Complex	1	2	1s	2s	3	4	4s	5	5s
U_{eff} / K	1835	1756	1873	1792	1815	1615	1653	1760	1757
τ_0 / s (10^{-12})	1.72	1.23	1.70	1.20	1.17	1.30	2.0	19.86	20.23
C (10^{-7})	7.05	6.71	7.06	6.73	10.0	10.0	100	16.64	678
n	3.44	3.60	3.45	3.61	3.77	3.90	5.0	2.15	1.25
T_B^{ZFC} / K	24	20	24	21	14	23	-	40	-
T_B^{100s} / K	17	15	17	15	12	19	10	56	53
T_B^{H} / K	23	23	25	25	9	22	22	60	30
H_C / T	1.9	1.8	1.9	1.8	0.5	1.7	1.3	2.0	0.4
M_r /μ_B	4.3	4.2	4.2	4.1	4.1	3.8	3.2	4.6	3.6

Results

Prediction of vibration modes for ligands

Herein, we studied the vibration spectra of ^{t}BuOH, HL_4 and a new alkoxide ligand with Ad group by DFT calculations (see Supplementary Materials). AdO^- was chosen due to its bulky Ad group consisting of a is highly symmetric and rigidly stable structure.[40] In the low energy regimes of 0-500 cm^{-1}, the calculating results show that the vibration modes of AdOH are much less compared to ^{t}BuOH and HL_4 (Fig. 1a). Nevertheless, the presence of low energy vibrational modes from these ligands essentially guarantee that some optical phonons of close-enough energy will couple with the spins and hence, affect relaxation at undesirable temperatures. In a real system, as these molecular motions occur, they also perturb the electric fields and subtly change the energies of individual $\pm m_J$ levels from that of the static model.[41,42]

Electronic structures for the complexes

We further study the electronic structures of two model complexes, namely $[Dy(1\text{-}AdO)_2(py)_5]BPh_4$ **1** and $[Dy(2\text{-}AdO)_2(py)_5]BPh_4$ **2** using the CASSCF/RASSISO/SINGLE-ANISO approach implemented in MOLCAS 8.0[43–45] (see Supplementary Materials). Similar to most of D_{5h} SMMs, *trans*-disposed $1\text{-}AdO^-$ and $2\text{-}AdO^-$

ligands confer a strong magnetic anisotropy to the central Dy^{III} ion. The main magnetic anisotropy axis is nearly collinear with the *pseudo* C_5 axis lying along the axial O–Dy–O orientation (see insert of Fig. 2a and 2b). For **1** and **2**, the ground state is highly anisotropic with m_J = |±15/2 > and $g_z \approx 20$. The other low-lying ligand field states (Table S6 and S7) follow the expected order of m_J = |±13/2>, |±11/2 > and |±9/2>, with relative energies of 584, 969, 1184 cm^{-1} for **1** and 563, 930, 1129 cm^{-1} for **2**, respectively, while the above subsequent excited states being highly mixed and bunched (Fig. 2). Using the average matrix elements of magnetic moment between the electronic states as a proxy for transition propensity (Table S10 and S11),[46,47] we speculate the most efficient magnetic relaxation pathway to occur via the highly bunched set of states which in this small biatomic entity the axial ligand field is purely axial, over 1248 to 1299 cm^{-1} for **1** and 1166 to 1225 cm^{-1} for **2**, which are consistent with experimentally determined U_{eff} (see below).

Simulations and analyses of molecular vibrations

The infrared spectra for the three complexes, namely **1** (as complex **2** is very similar to **1**, we take **1** as the representative to illustrate only), **3** and **4**, were calculated (Fig. 1b, see Supplementary Materials for details). As the low energy range of 0-500 cm^{-1} corresponds to the energy gaps between the ground and the first excited doublets in the electronic structures, this energy regime is especially considered. Certain groups of modes were chosen and the vibration vectors were expressed through VMD[48], which manifest that the vibrational shifts of the axial ligands in **1** are significantly smaller than the other molecules, especially the shift of alcohol oxygen atom in **1** is much minimized (Figs. 1c to 1e), indicating that the selection of rigid ligands increases the stiffness of the whole molecule (Fig. 1b and Figs S15 to S18). The calculated infrared spectra are in good agreement with the experimental results for **1** (Fig. S16) and **2** (Fig. S17), and the attribution of each peak to its vibration mode is listed in Table S15 and S16 (see also movies S1 to S11 for the motion of each movement). The vibration modes of specific groups correspond to strong and medium strong peaks in the wavelength range of the fingerprint (650–1350 cm^{-1}) and characteristic (above 1350 cm^{-1}) regions are showed in Fig. 3, which fit well to the experimental data and further prove the credibility of experimental measurements and theoretical simulations.

In addition,to ensure this prediction, the lattice vibration which correlates to the acoustic phonons was also considered. As all three molecules have the same space group, the displacement solution of tiny vibration in space can be described by Eq. 1, indicating that the vibration of lattice points is determined by the mass (m) of the unit.[49,50] While the molecular weights of **1** and **2** are larger than those of **3** and **4**, **1** and **2** should have the smallest lattice vibration. At this point, taking into account the intra- and inter-molecular vibrations, it is clear that rigid and bulky AdO^- ligand significantly stiffens the molecule.

$$u_i = \sum_j^{3N} \frac{a_{i,j}}{\sqrt{m_i}} A_j \cos\left(\omega_j t + \delta\right) \quad (1)$$

Syntheses of predicted complexes

As we have rich experience in engineering the equatorial-pyridine based D_{5h} symmetric Dy(III) SMMs[39,43] it is facile to displace the axial alcohol ligands with AdOH and the two desired complexes **1** and **2** are isolated in reasonable high yields. The synthetic procedure is detailed in the Materials and Methods section.

Crystal structures

Single crystal X-ray diffraction (Table S1) shows that the two cationic complexes $[Dy(AdO)_2(py)_5]^+$ (Fig. 4a) are very similar to previously reported other complexes belonging to the D_{5h} family[39,43]. Each asymmetric unit contains one central Dy^{3+} ion which is seven coordinated with five py molecules in the equatorial plane and two AdO^- ligands in the aixal position to form a pentagonal-bipyramidal geometry. The average Dy–O distances of 2.107(19) Å for **1** are little longer than that (2.110(3) Å) of **2**, and the five equatorial Dy–N bond lengths are similarly ranging from 2.55 to 2.60 Å for both complexes (Table S2). Indeed, the pentagonal-bipyramidal polyhedron is quite regular with an axial O–Dy–O angle of 173.77(7)° and 176.45(12)° for **1** and **2**, respectively; and five equatorial N–Dy–N angles ranging from 69.4(1)° to 73.4(1)° (Fig. 4b). CShM calculations of the Dy^{III} ions confirm a perfect D_{5h} local-symmetry (Table S3). From the space filling diagram of the asymmetric unit we can see the molecules are densely packed (Fig. 4c). However, except for van der Waals there is no other intermolecular interaction found, indicating the intermolecular interaction is weak. The shortest intermolecular Dy...Dy distance is 12.16(2) Å for **1** and 11.78(4) Å for **2** (Fig. S2 and S3), respectively.

Magnetic properties

As a whole, both complexes show similar paramagnetism in both solid and solution states. The temperature dependence of the magnetic susceptibilities were carried out under 1 kOe dc field in the temperature range of 2–300 K (Fig. S4), which gave the χT products (in the unit of $cm^3\ K\ mol^{-1}$) of 14.08 for **1**; 14.05 for **2** at 300 K. These values are very close to the expected value of 14.17 $cm^3\ K\ mol^{-1}$ for free Dy^{3+} ion. Upon cooling, the χT products for both complexes are essentially constant down to 50 K. At lower temperature, the χT products drop suddenly, indicating the onset of magnetic blocking (Fig. S4).

The field (H) dependence of the magnetization (M) for **1** and **1s** (Fig. 4); **2** and **2s** (Fig. S8) were measured at a 10 Oe/s sweeping rate. For **1** and **2** the magnetic hysteresis loops were not closed up to 23 K, which are in agreement with the zero-field-cooled (ZFC) and field-cooled (FC) magnetization measurements. Under a dc field of 1000 Oe the ZFC plots show a maximum at about 24 K for **1** (insert, Fig. 5d) and 20 K for **2** (Fig. S13). From the solution data of **1s** and **2s** we can see these peaks in the ZFC plots are nearly unchanged. We can even see a smaller step in zero dc field regime and slightly wider hysteresis loop at 2 K for **1s** compared to **1** (Fig. 5c). This feature is strikingly different to the previous examples[39,40], indicating the solution does not sabotage the magnetism of **1**, but even improve it. We reason that this is because the solution actually dilutes the sample of **1** and hence, reducing the QTM effect. Similar effect was also observed for **2** and **2s** (Fig. S14), indicating the adamantine group is really rigid regardless of the substitution positions because they are isomers.

Alternating current (ac) susceptibilities under zero dc field were measured for **1** and **2** (Fig. S5 and S6), and **1s** and **2s** (Fig. S10 and S11) at relatively high temperature range. The maxima of both the in-phase (χ') and out-of-phase (χ'') components showed a clear temperature dependence (Fig. S5). The frequency-dependent ac susceptibilities were also measured and the peaks of $\chi''(T)$ can be all observed from 40–98 K for **1** (Fig. 6a) and **2** (Fig. S6), similarly 40–98 K for **1s** and **2s** (Fig. 6a and Fig. S11) at the frequency ranging from 1 to 1218 Hz. And the frequency-dependent data can be fitted by a modified Debye function to obtain the Cole – Cole plots for **1** and **2** (Fig. S7) as well as for **1s** and **2s** (Fig. S12). All the α values are all less than 0.01 for **1** (Table S4), **2** (Table S5), **1s** (Table S6) and **2s** (Table S7), demonstrating narrow distributions of relaxation times for four samples. Figure 6b for **1** and fig. S13 for **2** are the plots of τ^{-1} versus T for the temperature dependent relaxation rate. The τ values are obtained by fitting the ac data with the equation $\tau^{-1} = {\tau_0}^{-1}e^{-U_{eff}/T} + CT^n$, giving the parameters summarized in Table 1. The U_{eff} value for **1** is slightly higher than that of **2**, owing to the little shorter Dy–O bonds. Overall, the high energy barriers of 1836(7) K for **1** and 1753(8) K for **2**, as well as high magnetic blocking temperatures (${T_B}^H$ = 23 K under an average sweep rate of 10 Oe/s and ${T_B}^{100s} \geq 15$ for both **1** and **2**) are observed as expected, which are among the top list of reported SMMs (Table 1 and Table S17). More strikingly, the ac dynamic magnetic properties of the solution samples (**1s** and **2s**) basically remain unchanged (${T_B}^H$ = 25 K under an average sweep rate of 10 Oe/s and ${T_B}^{100s} \geq 15$ K for both **1s** and **2s**) compared with their solid samples, indicating the molecule itself is rigid and stable enough, and the intermolecular interactions have nearly no effect on it. **1s** and **2s** also represent the best performance in the solutions of D_{5h} SMMs (Table 1 and Table S17).

Discussion

In brief, we have predesigned two high-performance D_{5h} Dy^{III} SMMs with rigid adamantanols in axial positions due to the much reduced vibration modes of the resulted complexes in low energy regimes. More strikingly, magnetic studies in both solid and solution states reveal almost unchanged dynamic behavior, indicating the use of high symmetry and rigidity ligands is successful to enhance the stiffness of the whole molecule and effectively suppress the quantum tunneling effect in solution. As vibration spectrometer is a common instrument in laboratories, we believe such a predesign method can become a general strategy for rationally constructing high-performance SMMs.

Methods

Materials

All chemicals were commercially available and were used as received. All the solvents were dehydrated and deoxygenated by Solvent Purification Systems prior to use. All manipulations were performed under a dry and oxygen-free argon atmosphere by using Schlenk techniques or in a glovebox.

Syntheses

For $[Dy(1\text{-}AdO)_2(py)_5][BPh_4]$ (1)

In an argon glovebox, reactants of $DyCl_3$ (0.5 mmol, 134 mg), 1-AdOH (1mmol, 156 mg) and $NaBPh_4$ (0.5 mmol, 171 mg) are added into about 8 mL THF in Schlenk tube and a cloudy solution forms. After stirring for 12 h at 85℃ oil bath, the cloudy solution is filtrated and the solvent of the filtrate is removed by vacuum to get a white powder of the solids. Then 2 mL pyridine is used to dissolve the white powders and filtrated the solution. Crystals suitable for X-ray diffraction are grown by slow diffusion of hexane to the saturated pyridine solution of **1** at room temperature for three days. Yield 226 mg, 36% (based on Dy). Elemental analysis calcd (%) for $C_{74}H_{81}N_6O_2DyB$: C 70.49, H 6.43, N 6.67; found: C 70.46, H 6.41, N 6.65. IR spectra (cm^{-1}): 2,905 s, 2,808 m, 2,716 w, 1,697 m, 1,568 m, 1,420 s, 1,120 s, 1,025 s, 1,002 m, 916 m, 743 m, 721 s, 687 s, 623 m, 521 w.

For [Dy(2-AdO)2(py)5][BPh4] (2)
The similar procedure as **1** is used to synthesize **2** with 1-AdOH replaced by 2-AdOH (1mmol,156mg). Yield 228mg, 35% (based on Dy). Elemental analysis calcd (%) for $C_{77}H_{88}N_6O_2DyB$: C 70.96, H 6.68, N 6.45; found: C 70.94, H 6.65, N 6.43. IR spectra (cm^{-1}): 2,907 s, 2,809 m, 2,718 w, 1,695 m, 1,564 m, 1,418 s, 1,123 s, 1,027 s, 1,004 m, 918 m, 745 m, 718 s, 683 s, 625 m, 518 w.

Solution preparation for 1s and 2s

125 mM solutions of **1** (**1s**) and **2** (**2s)** were prepared by dissolving block crystals of **1** (ca. 157mg) and **2** (ca. 163mg) in 1 mL pyridine, respectively, in an argon glovebox.

X-ray crystallography data

All data were recorded on a Bruker SMART CCD diffractometer with MoKα radiation (λ = 0.71073 Å). The structures were solved by direct methods and refined on F^2 using SHELXTL. CCDC 2073309 (**1**) and 2073311 (**2**) contain the supplementary crystallographic data for this paper mainly including Table S1–S3. These datas can be obtained free of charge via www.ccdc.cam.ac.uk/conts/retrieving.html (see Supplementary Materials).

Magnetic properties measurements

Magnetic susceptibility measurements have been carried out with a Quantum Design MPMS-XL7 SQUID magnetometer upon cooling from 300 to 2 K in variable applied fields. Ac susceptibility measurements have been performed at frequencies of between 1 and 1500 Hz with an oscillating field of 3.5 Oe and with variable dc applied field. Powder samples were embedded in eicosane to avoid any field induced crystal reorientation. Crystalline powders were fixed with eicosane, wrapped with film, and placed in the center of a straw. For the frozen solution sample **1s** and **2s**, a 125 mM pyridine solution of **1** and **2** were added into an NMR tube, which was sealed with paraffin, wrapped with Kapton tape, then the straw was put into magnetometer with the system temperature at 100 K in order to flash-freeze the solution. A diamagnetic correction has been calculated from Pascal constants and embedding eicosane has been applied to the observed magnetic susceptibility (see Supplementary Materials).

Electronic structure calculations

Ab initio calculations at SA-CASSCF/RASSI level were performed on program MOLCAS 8.0 and the structure was originally taken from the X-Ray structure. The basis sets were chosen from the ANO-RCC library as have been used in many works. The Dy atom was treated with VTZP quality, then the related B, C and O atoms with VDZP quality and others with VDZ quality. The state-averaged CASSCF orbitals of the sextets, quartets and doublets were optimized with 21, 224 and 490 states, respectively, with the RASSCF module. 21, 128 and 130 sextets, quartets and doublets chosen to construct and diagonalize in spin-orbit (SO) coupling Hamiltonian with the RASSI module. These computed SO states were written into the SINGLE_ANISO program to compute the g-tensors, crystal field parameters and magnetic energy levels for the doublets of the ground $J = 15/2$ multiple of the $^{6}H_{15/2}$ term for Dy(III). The two electron integrals were Cholesky decomposed with a threshold of 1×10^{-8} to account for the accuracy (see Supplementary Materials).

DFT calculations

In order to compare the molecular vibrations of distinctive compounds, we used Gaussian 09D to optimize their geometry and calculate their vibration frequencies. The element of dysprosium was substituted to yttrium to avoid convergence problem owing to the similar radius of their trivalent ions. Meanwhile, the atomic mass of yttrium was set as 162.5 (the natural abundance-weighted mass of dysprosium) to acquire more accurate harmonic vibrational modes. The geometry we used are from X-ray single crystal structure. The PBE density functional together with Grimme's D3 dispersion correction was employed in all calculations. We applied the cc-pVDZ basis set for carbon, hydrogen, oxygen, nitrogen and boron atoms, while for yttrium, the Stuttgart RSC 1997 effective core potential (ECP) was employed for its 28 core electrons and the rest of valence electrons were expressed using corresponding valence basis set (see Supplementary Materials).

Declarations

COMPETING INTERESTS

The authors declare no competing financial interests.

Corresponding Author

*zheng.yanzhen@xjtu.edu.cn

AUTHOR CONTRIBUTIONS

Y.-Z.Z. conceived and designed the experiments. X.-L.D. synthesized and characterized all the complexes. Y.-Q.Z. and Q.-C.L. analyzed magnetic and spectroscopy data, and carried out the *ab initio* and DFT calculations. X.-L.D., Y.-Q.Z., Q.-C.L. and Y.-Z.Z. wrote and revised the paper. X.-F.Z., Y.L., X.-L.Z. and C.K. provided the financial and technical support. All authors contributed in important discussions and suggestions on the manuscript.

ACKNOWLEDGEMENTS

This work was supported by NSFC (21871219, 21773130 and 21620102002), Key Laboratory Construction Program of Xi'an Municipal Bureau of Science and Technology (201805056ZD7CG40), the Shenzhen Science and Technology Program (JCYJ20180306170859634), and the Fundamental Research Funds for Central Universities. We also thank the Instrument Analysis Center of Xi'an Jiaotong University for the assistance from Dr. Gang Chang.

References

1. Leuenberger, M. N. & Loss, D. Quantum computing in molecular magnets. *Nature* **410**, 789–793 (2001).
2. Miyamachi, T. et al. Stabilizing the magnetic moment of single holmium atoms by symmetry. *Nature* **503**, 242–246 (2013).
3. Thiele, S. et al. Electrically driven nuclear spin resonance in single-molecule magnets. *Science* **344**, 1135–1138 (2014).
4. Gatteschi, D., Sessoli, R., & Villain, J. *Molecular nanomagnets*. (Oxford University Press, UK, 2006) Vol. 5.
5. Goodwin, C. A. P. et al. Molecular magnetic hysteresis at 60 kelvin in dysprosocenium. *Nature* **548**, 439–442 (2017).
6. Gould, C. A. et al. Synthesis and magnetism of neutral, linear metallocene complexes of terbium (II) and dysprosium (II). *J. Am. Chem. Soc.* **141**, 12967–12973 (2019).
7. Feltham, H. L. C. & Brooker, S. Review of purely 4f and mixed-metal nd-4f single-molecule magnets containing only one lanthanide ion. *Coord. Chem. Rev.* **276**, 1–33 (2014).
8. Liu, J.-L., Chen, Y.-C. & Tong, M.-L. Symmetry strategies for high performance lanthanide-based single-molecule magnets. *Chem. Soc. Rev.* **47**, 2431–2453 (2018).
9. Goodwin, C. A. P. Blocking like it's hot: a synthetic chemists' path to high-temperature lanthanide single molecule magnets. *Dalton Trans.* **49**, 14320–14337 (2020).
10. Wu, S.-G. et al. Field-induced oscillation of magnetization blocking barrier in a holmium metallacrown single-molecule magnet. *Chem.* **7**, 1–11 (2021).
11. Pedersen, K. S. et al. Toward molecular 4f single-ion magnet qubits. *J. Am. Chem. Soc.* **138**, 5801–5804 (2016).
12. Zhang, P. et al. Equatorially coordinated lanthanide single ion magnets. *J. Am. Chem. Soc.* **136**, 4484–4487 (2014).
13. Guo, F.-S. et al. Magnetic hysteresis up to 80 kelvin in a dysprosium metallocene single-molecule magnet. *Science* **362**, 1400–1403 (2018).
14. Boulon, M. E. et al. Magnetic anisotropy and spin-parity effect along the series of lanthanide complexes with DOTA. *Angew. Chem. Int. Ed.* **52**, 350–354 (2013).

15. Canaj, A. B. et al. Insight into D_{6h} symmetry: Targeting strong axiality in stable dysprosium(III) hexagonal bipyramidal single-ion magnets. *Angew. Chem. Int. Ed.* **58**, 14146–14151 (2019).
16. Vignesh, K. R. et al. Ferrotoroidic ground state in a heterometallic $\{Cr^{III}Dy^{III}_6\}$ complex displaying slow magnetic relaxation. *Nat. Commun.* **8**, 1023–1034 (2017).
17. Krylov, D. S. et al. Record-high thermal barrier of the relaxation of magnetization in the nitride clusterfullerene $Dy_2ScN@C_{80}$. *Chem. Commun.* **53**, 7901–7904 (2017).
18. Ungur, L. et al. Fine-tuning the local lymmetry to attain record blocking temperature and magnetic remanence in a single-ion magnet. *Angew. Chem., Int. Ed.* **53**, 4413–4417 (2014).
19. Liu, J.-L. et al. Switching the anisotropy barrier of a single-ion magnet by symmetry change from quasi-D_{5h} to quasi-O_h. *Chem. Sci.* **4**, 3310–3316 (2013).
20. Meihaus, K. R. & Long, J. R. Magnetic blocking at 10 K and a dipolar-mediated avalanche in salts of the bis (η-cyclooctatetraenide) complex $[Er(COT)_2]^-$. *J. Am. Chem. Soc.* **135**, 17952–17957 (2013).
21. Rinehart, J. D. & Long, J. R. Exploiting single-ion anisotropy in the design of f-element single-molecule magnets. *Chem. Sci.* **2**, 2078–2085 (2011).
22. Parmar, V. S. et al. Probing relaxation dynamics in five-coordinate dysprosium single-molecule magnets. *Chem. Eur. J.* **26**, 7774–7778 (2020).
23. Jiang, S.-D. et al. A mononuclear dysprosium complex featuring single-molecule-magnet mehavior. *Angew. Chem., Int. Ed.* **49**, 7448–7451 (2010).
24. Chen, Y.-C. et al. Symmetry-supported magnetic blocking at 20 K in pentagonal bipyramidal Dy(III) single-ion magnets. *J. Am. Chem. Soc.* **138**, 2829–2837 (2016).
25. Liu, J. et al. A stable pentagonal bipyramidal Dy(III) single-ion magnet with a record magnetization reversal barrier over 1000 K. *J. Am. Chem. Soc.* **138**, 5441–5450 (2016).
26. Ding, Y.-S. et al. Field-and temperature-dependent quantum tunnelling of the magnetisation in a large barrier single-molecule magnet. *Nat. Commun.* **9**, 1–10 (2018).
27. Spree, C. et al. Single-molecule magnets $DyM_2N@C_{80}$ and $Dy_2MN@C_{80}$(M = Sc, Lu): The impact of diamagnetic metals on Dy^{3+} magnetic anisotropy, Dy···Dy coupling, and mixing of molecular and lattice vibrations. *Chem. Eur. J.* **26**, 2436–2449 (2020).
28. *Rinehart*<bi>,</bi> *J. D.*<bi>,</bi> *Fang*<bi>,</bi> *M.*<bi>,</bi> *Evans*<bi>,</bi> *W. J.* & *Long*, *J. R.* Strong exchange and magnetic blocking in N_2^{3-}-radical-bridged lanthanide complexes. *Nat. Chem.* **3**, 538–542 (2011).
29. Ma, Y.-J. et al. Manipulating on/off single-molecule magnet behavior in a Dy(III)-based photochromic complex. *J. Am. Chem. Soc.* **142**, 2682–2689 (2020).
30. Zhu, Z., Guo, M., Li, X.-L. & J. Tang, Molecular magnetism of lanthanide: Advances and perspectives. *Coord. Chem. Rev.* **378**, 350–364 (2019).
31. Chilton, N. F. et al. Single molecule magnetism in a family of mononuclear β-diketonate lanthanide(III) complexes: rationalization of magnetic anisotropy in complexes of low symmetry.

Chem. Sci. **4**, 1719–1730 (2013).

32. Yu, K.-X. et al. Enhancing magnetic hysteresis in single-molecule magnets by ligand functionalization. *Chem.* **6**, 1777–1793 (2020).
33. Chen, Y.-C. et al. Hyperfine-interaction-driven suppression of quantum tunneling at zero field in a Holmium(III) single-ion magnet. *Angew. Chem., Int. Ed.* **56**, 4996–5000 (2017).
34. Katoh, K. et al. Control of the spin dynamics of single-molecule magnets by using a quasi one-dimensional arrangement. *Angew. Chem. Int. Ed.* **57**, 9262–9267 (2018).
35. Wang, H. et al. Single-molecule magnetism of tetrapyrrole lanthanide compounds with sandwich multiple-decker structures. *Coord. Chem. Rev.* **306**, 195–216 (2016).
36. Moutet, J. et al. Bis-cyclooctatetraenyl Thulium(II): Highly reducing lanthanide sandwich single-molecule magnets. *Angew. Chem. Int. Ed.* **133**, 6107–6111 (2021).
37. Ding, Y.-S. et al. On approaching the limit of molecular magnetic anisotropy: a near-perfect pentagonal bipyramidal dysprosium (III) single-molecule magnet. *Angew. Chem. Int. Ed.* **55**, 16071–16074 (2016).
38. Gao, C. et al. Observation of the asphericity of 4f-electron density and its relation to the magnetic anisotropy axis in single-molecule magnets. *Nat. Chem.* <background-color:#FFCC66;bu>12</background-color:#FFCC66;bu>, 213–219 (2020).
39. Sheehan, B. C. et al. Direct spectroscopic observation of berry-phase interference in the Ni_4 single-molecule magnet. *Phys. Rev. B* **102**, 224428 (2020).
40. Dipl, H. S., Fokin, A. A. & Schreiner, P. R. Diamonds are a chemist's best friend: diamondoid chemistry beyond adamantane. *Angew. Chem., Int. Ed.* **47**, 1022–1036 (2008).
41. Reta, D. & Chilton, N. F. Uncertainty estimates for magnetic relaxation times and magnetic relaxation parameters. *Phys. Chem. Chem. Phys.* **21**, 23567–23575 (2019).
42. Chiesa, A. F. et al. Understanding magnetic relaxation in single-ion magnets with high blocking temperature. *Phys. Rev. B* **101**, 174402 (2020).
43. Aquilante, F. et al. Molcas 8: New capabilities for multiconfigurational quantum chemical calculations across the periodic table. *J. Comput. Chem.* **37**, 506 (2016).
44. Chibotaru, L. F. & Ungur, L. Ab initio calculation of anisotropic magnetic properties of complexes: Unique definition of pseudospin Hamiltonians and their derivation. *J. Chem. Phys.* **137**, 064112 (2012).
45. Granovsky, A. A. Extended multi-configuration quasi-degenerate perturbation theory: The new approach to multi-state multi-reference perturbation theory. *J. Chem. Phys.* **134**, 214113 (2011).
46. Liu, B.-C. et al. An imido ligand significantly enhances the effective energy barrier of dysprosium(III) single-molecule magnets. *Chem. Commun.* **55**, 9355–9358 (2019).
47. Ding, X.-L. et al. A local D_{4h} symmetric dysprosium(III) single-molecule magnet with an energy barrier exceeding 2000 K. *Chem. Eur. J.* **27**, 2623–2627 (2021).

48. Humphrey, W. Dalke, A. & Schulten, K. VMD: visual molecular dynamics. *J. Mol. Graphics.* **14**, 33–38 (1996).
49. Gu, L. & Wu, R. Origins of slow magnetic relaxation in single-molecule magnets. *Phys. Rev. Lett.* **125**, 117203 (2020).
50. Gu, L. & Wu, R. Origin of the anomalously low Raman exponents in single molecule magnets. *Phys. Rev. B* **103**, 014401 (2021).

Figures

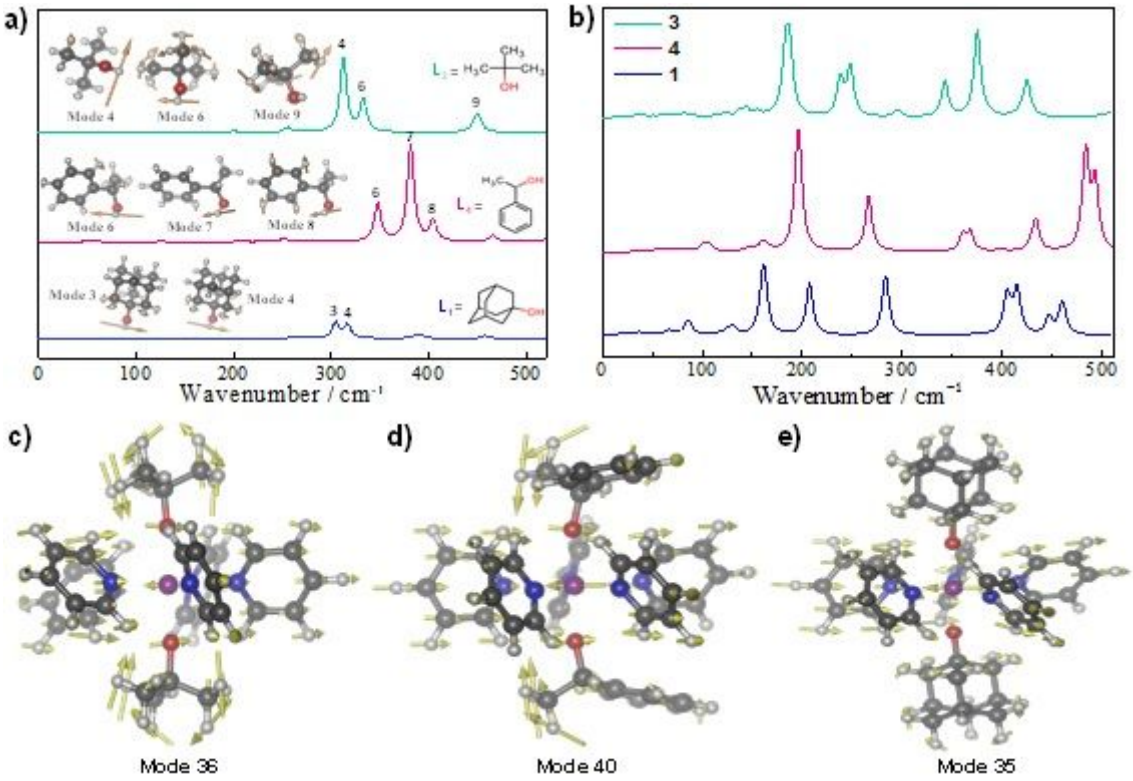

Figure 1

(a and b) Calculated vibration spectra for the axial ligands and the cations in 1, 3 and 4 at low energy regime. (c, d and e) The atomic motion patterns under similar vibration modes for the cations of 1, 3 and 4; the orientations and lengths of the arrows represent the directions and strengths of the molecular vibration vectors, respectively. Color codes: purple for Dy, red for O, gray for C, blue for N, and white for H.

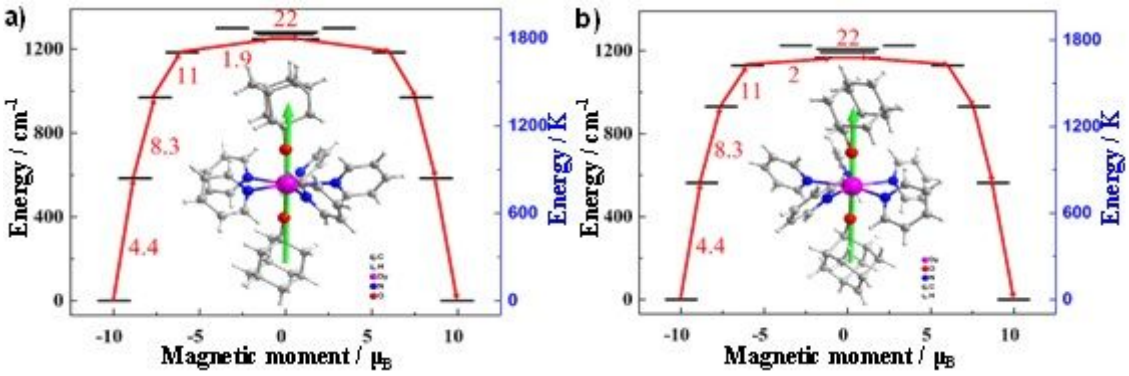

Figure 2

Ab initio calculated electronic states of the J = 15/2 manifold of the 6H15/2 term of DyIII in 1 (a) and 2 (b). The principal magnetic axis of the ground Kramer's doublets of 1 and 2 are inserted in a and b, respectively. The arrows show the connected energy states with the number representing the matrix elements of the transverse magnetic moments (see text for details). The black line indicates the KDs as functions of the magnetic moments. The red arrow indicates the magnetic relaxation pathways. The numbers above each arrow represent the corresponding transverse matrix elements.

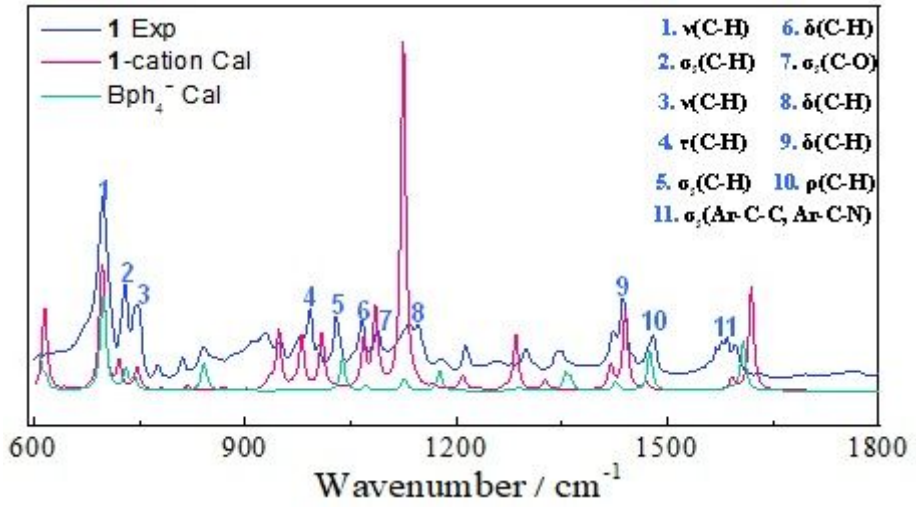

Figure 3

Experimental and simulated infrared spectra for 1. The blue line represents the experimental curve; the red and green lines are the calculated spectra for its cation and anion components, respectively.

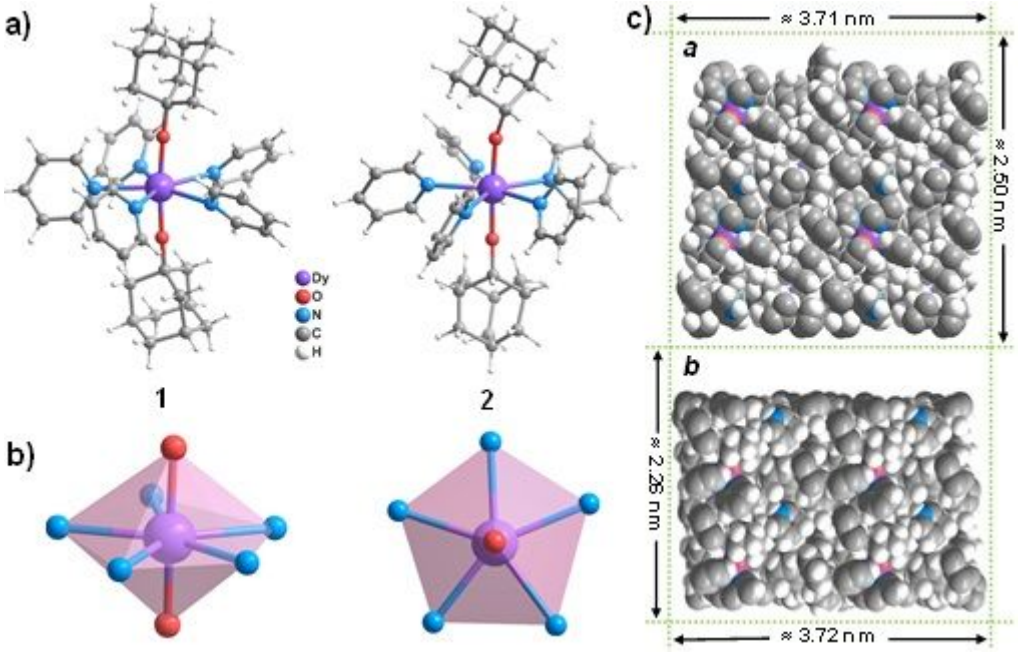

Figure 4

Crystal structure diagrams for the complexes. (a) The molecular structures of the [Dy(AdO)2(py)5]+ cations in 1 and 2; other atoms are omitted for clarify. (b) The polyhedron of the DyIII ions viewed from the front (left) and the top (right). (c) The space filling diagram viewed along a and b axis for 1 framed in one asymmetric unit cell.

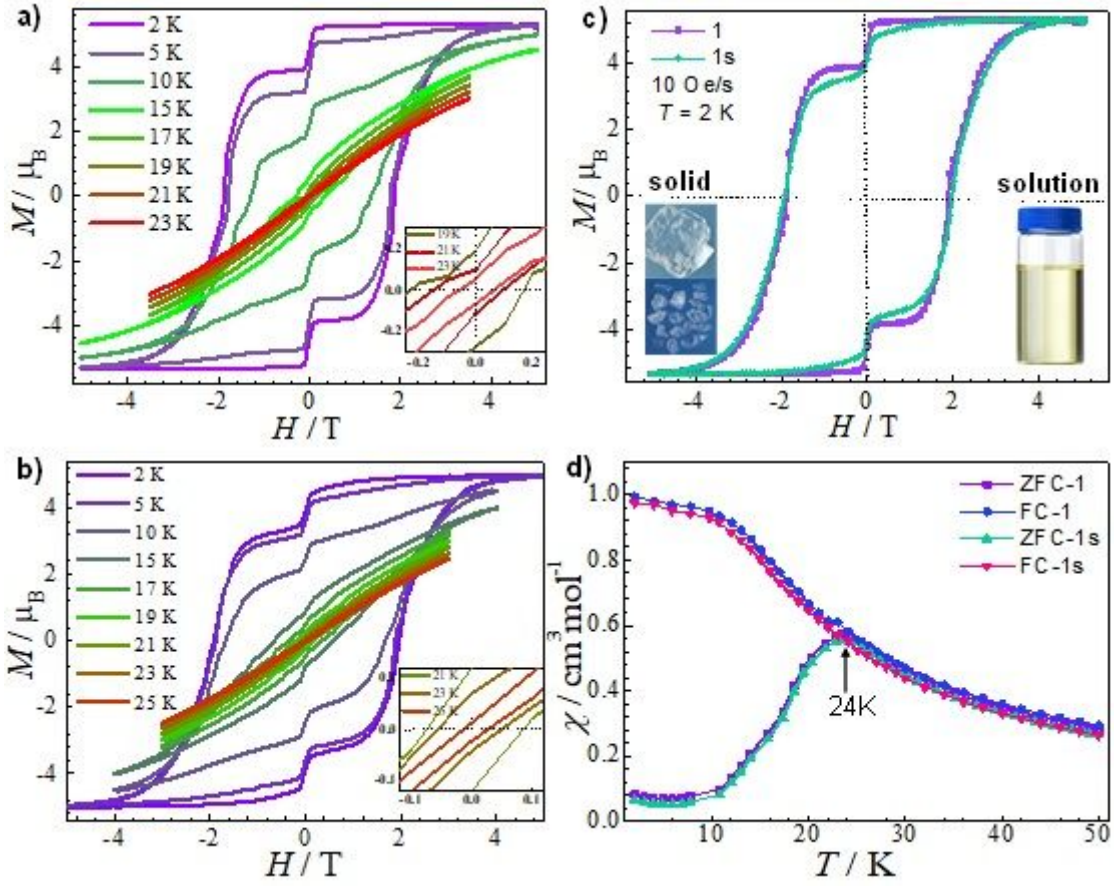

Figure 5

(a and b) Magnetic hysteresis loops for 1 (solid state) and 1s (solution state) under an average sweep rate of 10 Oe/s. (c) A comparison of the magnetic hysteresis at 2 K for 1 and 1s. (d) Field-cooled (FC) and zero-field-cooled (ZFC) magnetic susceptibilities of 1 and 1s measured under a dc field of 1000 Oe.

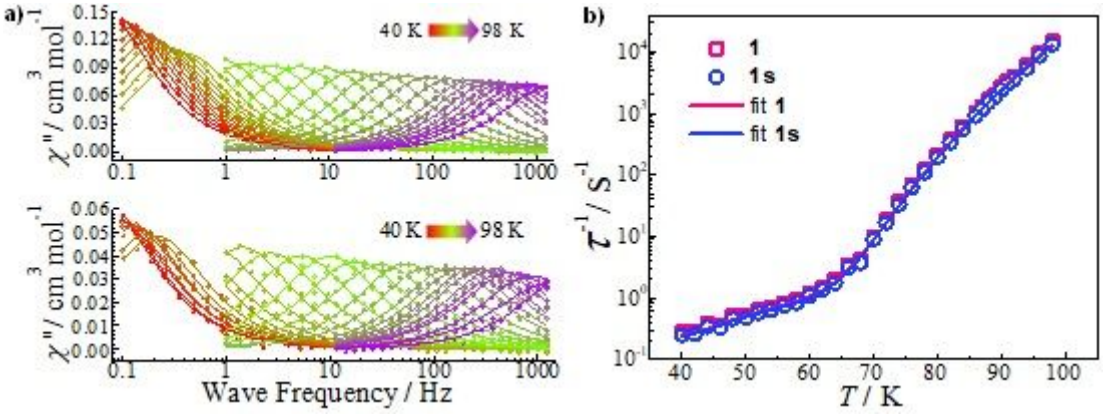

Figure 6

(a) The frequency-dependent ac susceptibilities from 40-98 K at 0.1-1218 Hz for 1 (top) and 1s (bottom). (b) Temperature dependence of the relaxation time τ in a zero dc field for 1 and 1s, the solid lines are the best fits

Supplementary Files

This is a list of supplementary files associated with this preprint. Click to download.

- SINat.Com.pdf
- Movies.mp4